Computer modelling of B_2O_3. II. Molecular dynamics simulations of vitreous structures

1995 J. Phys.: Condens. Matter 7 8693

(http://iopscience.iop.org/0953-8984/7/46/004)

J. Phys.: Condens. Matter 7 (1995) 8693–8722. Printed in the UK

Computer modelling of B_2O_3: part II. Molecular dynamics simulations of vitreous structures

Akira Takada†‡‖, C R A Catlow† and G D Price§

† Davy Faraday Research Laboratory, Royal Institution of Great Britain, 21 Albemarle Street, London W1X 4BS, UK

‡ Fundamental Research Laboratory, Asahi Glass Co. Ltd., 1150 Hazawa-cho, Yokohama 221, Japan

§ Research School of Geological and Geophysical Sciences, Birkbeck College and University College London, Gower Street, London W1E 6BT, UK

Received 1 June 1995

Abstract. We use our recently developed interatomic potential, which can reproduce the crystal structures of both phases of B_2O_3, in a molecular dynamics study of the structures of vitreous B_2O_3. Our calculated results suggest that the use of a partial charge model, and the inclusion of a B–O–B bond-bending, three-body term are important in reproducing the structure of this vitreous material. They also demonstrate the presence of boroxol (six-membered) rings in the simulated structures. Improved results are obtained when the potentials are refined by the inclusion of coordination-dependent terms which result in a higher proportion of boroxol rings in accordance with experimental data.

1. Introduction

There is a long-standing controversy concerning the structure of vitreous B_2O_3 [1]. Moreover, the development of adequate theoretical models of its structure is difficult due to the complexity of boron–oxygen bonding, which is not only partially covalent, but also allows the boron coordination number to change depending on its environment. Several interatomic potentials have been reported for the study of vitreous structures of B_2O_3. However, there have been no previous attempts to model the crystal structures of B_2O_3 and apply the resulting interatomic potentials to the vitreous structures. A key feature of our approach is that it is essential for any potential model to reproduce crystal structures and to this end part I of this study has reported different models developed by fitting to *ab initio* quantum mechanical data, within the restraints imposed by the experimental crystal structures. In the next section of this paper we review previous simulation studies of vitreous B_2O_3. We then present the models developed using our new interatomic potentials for this material, which for the first time are able to simulate the formation in the material of a considerable proportion of boroxol rings. Finally, we discuss how features of our interatomic potentials influence the simulated structures.

‖ Author to whom any correspondence should be sent.

0953-8984/95/468693+30$19.50

2. Experimental and computational background

2.1. Structure of vitreous boric oxide and borates

The random-network model, proposed by Zachariasen [2] is amongst the best known models for the structures of glassy materials. For example, in vitreous silica, SiO_4 tetrahedra provide the framework (network-former), in which the silicon atom is tetrahedrally surrounded by four oxygen atoms and each oxygen atom is bonded to two silicon atoms. Although the first coordination shell is the same as that of the crystalline structure, the tetrahedra are rearranged in a non-periodic manner in three dimensions. For boric oxide glass, the simpler random-network model consists of planar BO_3 triangles, as also proposed by Zachariasen [2]. However, several serious objections to this model have been raised, as reviewed in the volume of proceedings edited by Pye *et al* [1] and also by Johnson [3].

Since Zachariasen's model [2] was published, several rules concerning vitreous structures of borates [4–6] have been formulated (although subsequently challenged) and several structural models have been proposed. Historically, the field has developed from the random-network model (containing no boroxol rings [2]) to the boroxol ring model [7] the quasicrystalline model [8], while models based on the B_4O_6 molecule [9] have also been proposed (see figure 1). From the considerable amount of data accumulated and analysed, the former two models are now favoured.

As for the coordination of boron in vitreous B_2O_3, the hypothesis that almost all the borons have threefold coordination is supported by all the experimental data and is widely accepted (although in view of the coordination change from the threefold-coordinated triangle (BO_3) to a fourfold-coordinated tetrahedron (BO_4) in binary alkaline borate glasses a change in the coordination number has been invoked in order to explain so-called 'boron oxide anomaly' [1]). However, the mode of connecting the BO_3 triangles is still controversial. Goubeau and Keller [10] first suggested the existence of boroxol groups in B_2O_3 glass in order to explain the extremely sharp line at 808 cm^{-1} in the Raman spectrum. Krogh-Moe [7] analysed NMR, infrared and Raman spectroscopic, x-ray diffraction, density, energy and viscosity data. He concluded that a random three-dimensional network of BO_3 triangles with a comparatively high fraction of boroxol rings gives the best explanation of the available data.

In contrast, Elliot [11] claimed that the continuous random-network (CRN) model containing no boroxol rings, modified from the structure of threefold-coordinated amorphous arsenic, can reproduce the radial distribution functions of the x-ray study of Mozzi and Warren [12]. However, the problem with this model is that the density is some 30% lower than that observed experimentally.

The boroxol ring model has, however, the same problems. Although it can give a satisfactory account of the radial distribution function (RDF) obtained from the x-ray diffraction data at small interatomic separations, it does not necessarily reproduce the measured density correctly [13]. Bell and Carnevale [13] proposed a locally layered random-network model, in which adjacent layers are weakly bonded by the occasional overlapping of boroxol rings rotated relative to each other by 60° although, as discussed in the previous paper, such structures do not appear to be stable.

To summarize, a wide range of experimental data favour the boroxol ring model. However, there is no conclusive evidence for rejecting the continuous random-network model containing no such rings. However, all the above approaches based purely on topological considerations seems to have serious limitations. More detailed models are required.

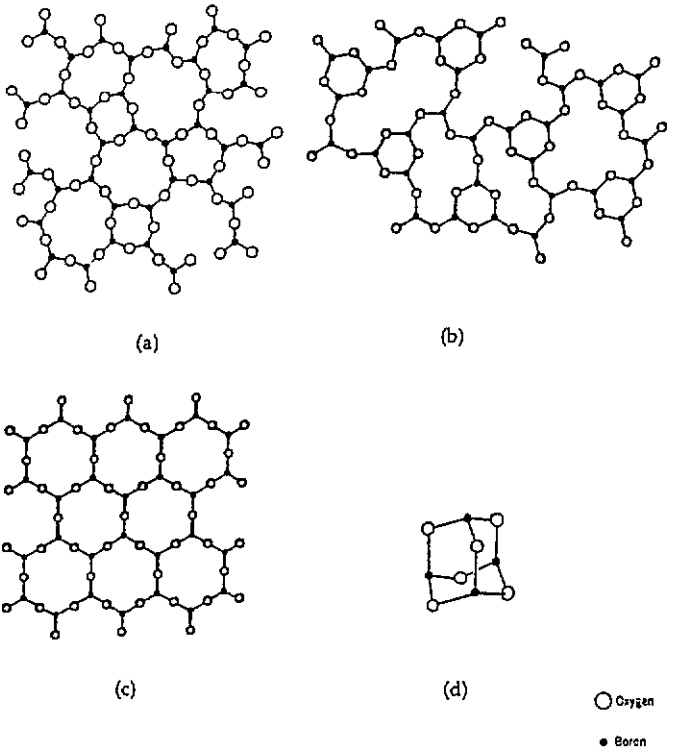

Figure 1. Schematic representation of the structural models of vitreous boric oxides [7]: (a) the random-network model; (b) the boroxol ring model; (c) the quasicrystalline model; (d) the B_4O_6 molecule model.

2.2. Previous molecular dynamics simulation studies

Since the pioneering study of Woodcock *et al* [14] on the simulation of vitreous silica, molecular dynamics (MD) simulations have been recognized as a powerful tool in studying structural and rheological properties of glasses. However, compared to the several studies of silicates, there are few investigations of borate glasses; and in all reported simulations of vitreous B_2O_3 there are discrepancies between experimental data and simulations.

The first modelling studies of borate glasses were initiated by Soules [15, 16] and Soules and Varshneya [17]. They calculated the structures of vitreous B_2O_3 and sodium borosilicate glass. They showed that in vitreous B_2O_3 boron atoms are trigonally coordinated to oxygen atoms, while in sodium borosilicate glasses the trigonal to tetrahedral conversion of boron atoms accompanies the addition of sodium atoms. These two aspects of their results agree well with the experimental data. However, no boroxol group formation is observed in their simulations.

A series of more detailed studies were carried out by Soppe *et al* [18] and Soppe and den Hartog [19, 20]. They consistently failed to find any boroxol rings in their simulation studies. Their studies of both non-pressure-scaled and pressure-scaled systems, with a variety of different quench rates, found no tendency for oxygen to become co-planar in adjacent BO_3 triangles. They also attempted an interesting simulation in which half of the B–O–B and O–B–O angles were constrained at 120° . Even with such artificial constraints, boroxol rings still do not form in their structures. They concluded that their continuous

random-network structure without any boroxol rings reasonably reproduced the RDF of the x-ray data. Similar results were obtained by Amini *et al* [21], Abramo *et al* [22], Xu *et al* [23] who also performed MD simulations on B_2O_3, and on silver borate and sodium borate glasses. Again no boroxol groups were found in the simulated structures.

All of these studies have two limitations. The first is that very rapid quenching rates have to be used. Slow processes such as quenching (quenching rates in the real process are less than 10^3 K s^{-1}) technically cannot be simulated by MD, so artificially much higher quenching rates (10^{13}–10^{15} K s^{-1}) are normally used in computer simulations. However, despite the use of such quench rates, several simulations of silica glass have succeeded in reproducing the structures of the vitreous material. The second limitation is the use of pair-potential models with formal charges. Pair-potential models have succeeded in modelling many ionic materials. However, such pair-potentials may not be sufficient to express the structure and bonding of materials like B_2O_3 with a high degree of covalency, as shown in the previous paper.

In order to account for covalency, Hirao and Soga [24] applied a new potential with an extra attractive exponential form for B–B interactions to sodium borate glasses. The calculated population of B–O–B angles at ~120° indicates the presence of boroxol groups. The MD study of Inoue *et al* [25] which included three-body effects is the only one that generates both boroxol rings in B_2O_3 glass and diborate groups in sodium borate glass. They put ghost atoms (G) on the 'centroid' of both BO_2 and B_2O triangles. A positive point charge with a Born–Mayer-type short-range potential is assumed to exist at G when the G–O potential is calculated, and a negative point charge with a different Born–Mayer-type short-range potential when the G–B potential is calculated. These ghost atoms thus provide O–B–O and B–O–B three-body potentials. Boron and oxygen atoms have formal charges, and all the other potential parameters are derived from the potential energy of H_3BO_3 by the INDO (intermediate neglect of differential overlap) method.

They concluded that their 'pseudo-atom' three-body type of model reproduces the RDF of Mozzi and Warren [12] with the presence of boroxol rings. However, the ratio of boron atoms present in the boroxol rings is less than 22.5% and smaller than that reported ($82 \pm 8\%$ by Jellison *et al* [26] and $60 \pm 20\%$ by Johnson *et al* [3]). This result is encouraging in that it shows that structures with boroxol rings can be reproduced by three-body potentials, even if a rapid quench rate is used. It is, moreover, interesting to note that calculated B–O–B bond angles are distributed around 120°. In contrast, all pair-potential studies show B–O–B angles of ~160°. The NMR data of Jellison *et al* [26] give information on the B–O–B angles for oxygen atoms not included in boroxol rings. The NMR result shows a narrow distribution centred around either 134.6° or 128.1°, close to the value of 130° used by Mozzi and Warren [12].

Recently Verhoef and den Hartog [27] carried out MD simulations of B_2O_3 glass, using different sets of pair-potentials (of the Born–Mayer–Huggins type) and in some cases three-body, bond-bending terms were applied. For the latter a simple harmonic form was used. The equilibrium angle was set as 120° for O–B–O and 130° for B–O–B. The force constant for O–B–O was fixed so as to obtain the correct energy for the high-frequency mode in the simulated infrared spectrum.

Their first conclusion is that all the models investigated generate continuous random-network glass structures without any boroxol rings, even if three-body bond-bending terms are added. All their models reproduce the experimental data reasonably well, although there are detailed discrepancies mainly within the distance range of 2–4 Å in the RDF. Their third conclusion is that the peak at 806 cm^{-1} in the experimental Raman spectra can be assigned to a breathing mode of the three oxygen atoms within each BO_3 triangle.

However, no peak at around 806 cm^{-1} is observed experimentally in borate crystals which consist of BO_3 triangles. Finally, they conclude that three-body interactions are necessary to reproduce the high-frequency modes in the simulated infrared spectra and density of state.

Thus, we can now summarize the results of all these MD simulations:

(i) Pair-potential models can reproduce the RDFs derived from short- range data for x-ray and neutron scattering well at short distances. However, discrepancies remain for medium range distances. B–O–B angles are far from the average experimental values of 130° estimated from NMR data. Pair-potential models always generate continuous random networks without any boroxol rings.

(ii) Three-body potential models can generate structures containing boroxol rings (although this is not always the case). They can reproduce some characteristics of the medium-range order which are similar to Mozzi and Warren's model. The inclusion of the three-body potential affects not only the generation of boroxol rings but also the vibrational properties of the simulated vitreous material.

The work reported later in this paper will use new improved descriptions of the interatomic potential models for B_2O_3 and will achieve considerably better agreement with experiment as compared with the results discussed above.

3. Computational model

3.1. Use of transferable potential

3.1.1. Potential model for MD simulation. We have already developed a transferable potential model for crystalline B_2O_3 in part I of this study. We recall that this model was derived in order to reproduce both crystalline structures [28, 29] of B_2O_3 where one structure has threefold and the other has fourfold-coordinated boron atoms (see figures 1 and 2 in part I of this study).

We used the Buckingham potential plus Coulombic term for the O–O and the B–B interactions:

$$V(r_{ij}) = A\exp(-r_{ij}/\rho_{ij}) - Cr_{ij}^{-6} + q_iq_j/r_{ij} \tag{1}$$

and the Morse potential plus Coulombic term for the B–O interaction:

$$V(r_{ij}) = D_{ij}\{1 - \exp[-\beta_{ij}(r_{ij} - r_0)]\}^2 + q_iq_j/r_{ij}. \tag{2}$$

In order to express more covalent effects, a three-body term was added. The form used is the simple-harmonic, bond-bending form:

$$V(\theta) = \tfrac{1}{2}K_B(\theta - \theta_0)^2 \tag{3}$$

where K_B is the bond-bending force constant and θ_0 is the equilibrium bond angle.

The potential B1 (named in part I of this study) was chosen among several transferable potential sets, because the crystal structures calculated using this potential set were investigated in detail and proved to be reproduced better. The parameters for the applied potential and the crystal structures, which were calculated using this potential, are listed in part I of this study. We note that straightforward implementation of the 'coordination-dependent' potentials C1 and C2 is not possible in MD simulations, although we report a modified procedure late in this paper.

We now apply potential model B1 to the simulated melting and quenching of the B_2O_3 crystal employing MD techniques [30]. Our MD calculations are performed employing the modified version of the code FUNGUS. The details of the code were reported elsewhere

Table 1. Distribution of coordination numbers in the calculated glass.

	Onefold	Twofold	Threefold	Fourfold
(i) Constant-pressure calculations using potential B1				
Potential	**B1**			
Boron	0%	0%	96%	4%
Oxygen	0%	97%	3%	0%
(ii) Constant-pressure calculations using modified potentials C1 and C2				
Potential	**C1**			
Boron	0%	1%	99%	0%
Oxygen	1%	99%	0%	0%
Potential	**C2**			
Boron	0%	1%	99%	0%
Oxygen	2%	96%	2%	0%
(iii) Constant-volume calculations using modified potentials C1 and C2				
Potential	**C1**			
Boron	0%	1%	99%	0%
Oxygen	1%	98%	1%	0%
Potential	**C2**			
Boron	0%	0%	94%	6%
Oxygen	4%	89%	7%	0%

[31, 32]. This code uses a periodic boundary condition to simulate the behaviour of an infinite system. The long-range Coulombic interactions are computed using Ewald's method [33]. The program can be used for potential models which include three-body, bond-bending-type interactions. Here we have also added the four-body potential terms in order to retain planarity of the BO_3 triangle, and moreover the pair-potential terms whose parameters are automatically modified depending on the coordination numbers.

3.1.2. Results of simulations with transferable potential. We now apply potential B1 to simulating the melting and quenching of B_2O_3 into the vitreous state. The conditions used in the calculations are as follows. The total number of atoms in the periodic repeated simulation box was 480 (192 boron atoms and 288 oxygen atoms) and the time step was 1 fs. When we started our MD simulations, two problems occurred. The first was that when the system was heated to a temperature higher than 1500 K in the constant-pressure calculations using ambient pressures, the simulation box expanded to become several times larger than the original size and reasonable dimensions could not be restored. The second was that when the constant-volume method was used, a large fraction of fourfold-coordinated boron atoms was generated, which remained even at the 300 K. The size of simulation box will clearly influence simulated structures and it is evidently desirable to be able to reproduce the experimental density using ambient pressures. It appears that up to a temperature of 1500 K bonds can be broken and remade, resulting in the reproduction (approximately) of the density of the molten state. Therefore, we adopted the constant-pressure method using ambient pressures with a maximum temperature of 1500 K in order to prevent the disruption of the simulation box and the generation of fourfold-coordinated boron atoms.

The detailed procedure was as follows. The crystal of B_2O_3-I was kept at 1500 K for 10 000 steps. The system was then quenched down to 300 K in 100 K intervals each of 3000 steps and kept at 300 K for 10 000 steps. This melting and quenching process was repeated

once more. To check the rate of atomic diffusion during the melting, the rate of disruption of the B–O bonds was counted. In this case, 17% of the initial bonds were broken and rebonded with another partner. Although the atomic diffusion is small, it is encouraging that the simulation reproduced the density of the molten state. The calculated results, however, have revealed weaknesses with potential B1, mentioned later in this section, and therefore it was not useful to run the simulations for longer. Studies of systems with more appropriate potentials in which there has been considerably greater diffusion will be reported in section 3.3.

Table 2. Distribution of ring sizes in the calculated glass.

Ring size	4	6	8	10	12
(i) Total number of atoms is 480; constant-pressure calculations using potential B1					
Potential	**B1**				
Number	1	17	5	9	14
(ii) Total number of atoms is 270; constant-pressure calculations using modified potentials C1 and C2					
Potential	**C1**				
Number	0	13	3	0	2
Potential	**C2**				
Number	2	19	4	2	2
(iii) Total number of atoms is 270; constant-volume calculations using modified potentials C1 and C2					
Potential	**C1**				
Number	0	9	8	2	9
Potential	**C2**				
Number	0	15	7	5	10

Table 3. Experimental and calculated densities. Constant-pressure calculations using potentials B1, C1 and C2.

	300 K crystal ($g\ cm^{-3}$)	1500 K melt ($g\ cm^{-3}$)	300 K glass ($g\ cm^{-3}$)
Experimental[a]	2.56	1.51	1.80
Calculation			
Potential B1	2.55	1.52	1.63
Potential C1	2.51	—	1.43
Potential C2	2.53	—	1.15

[a] From [34].

The calculated coordination numbers, ring sizes, and densities are given in tables 1–3. The results show that 17 six-membered rings, were generated (that is, 27% of the boron atoms are present in six-membered rings), although the proportion is smaller than that estimated experimentally ($82 \pm 8\%$ by Jellison *et al* [26]; $60 \pm 20\%$ by Johnson *et al* [3]). It is interesting to note that even the ambient pressure simulation gave a reasonable density, in contrast to most of the published constant-pressure calculations which require extremely high pressures in order to reproduce the experimental density.

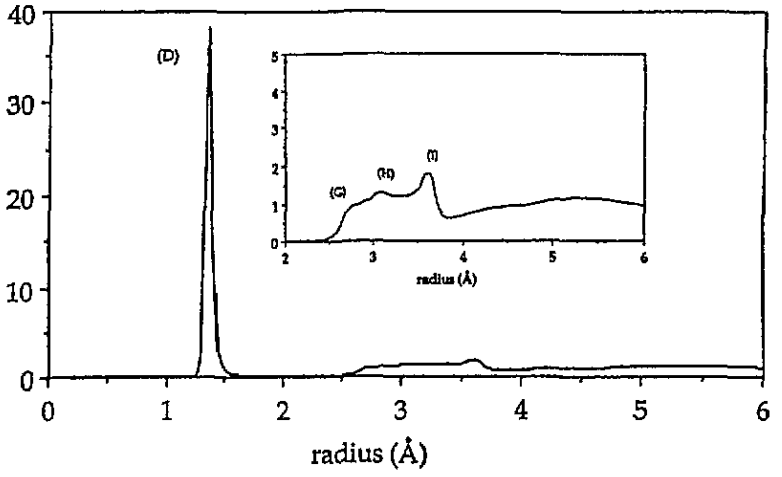

Figure 2. The calculated B–O PDF for glass at 300 K (using potential B1). See figure 6 for assignments of (D), (G), (H) and (I).

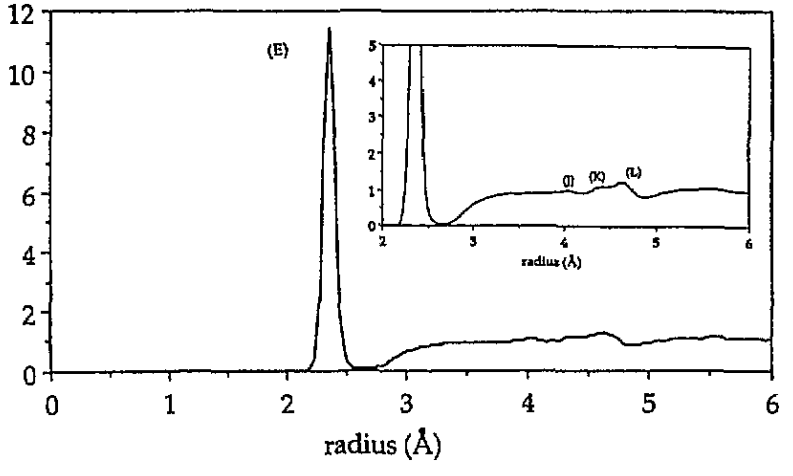

Figure 3. Calculated O–O PDF for glass at 300 K (using potential B1). See figure 6 for assignments of (E), (J), (K) and (L).

The pair distribution functions (PDFs) and the bond angle distributions (BADs) are shown in figures 2–5. The assignments of the peaks by Mozzi and Warren are shown in figure 6 [12]. Although the volume of the simulation box expanded by about 10% in the ambient pressure simulation, the positions of the peaks of B–O, O–O and B–B are reasonable. It is interesting to note that there are several peaks (for example, G and H) which suggest the existence of boroxol rings and which are not present in the calculated results based on pair potentials. There is also a major difference in the BADs. All the pair-potential models exhibited a broad distribution of the B–O–B bond angles around $\approx 160°$, while the present calculations show a sharp distribution around $120 \sim 130°$. As explained in part I of this study, accurate B–O–B bond angles are essential for reproducing the crystal structure of B_2O_3-I, and they also seem important in the case of the vitreous structures. The average B–O–B bond angle in the borate crystals is approximately 130° and the quantum-chemical calculations on the molecular clusters suggested a value of around

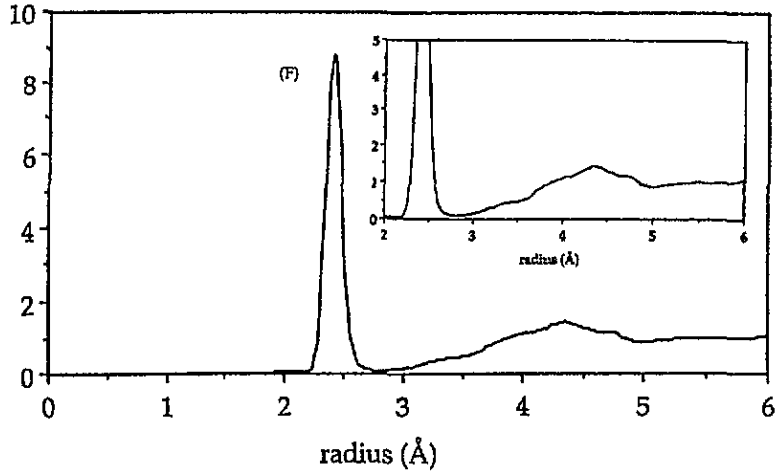

Figure 4. Calculated B–B PDF for glass at 300 K (using potential B1). See figure 6 for assignment of (F).

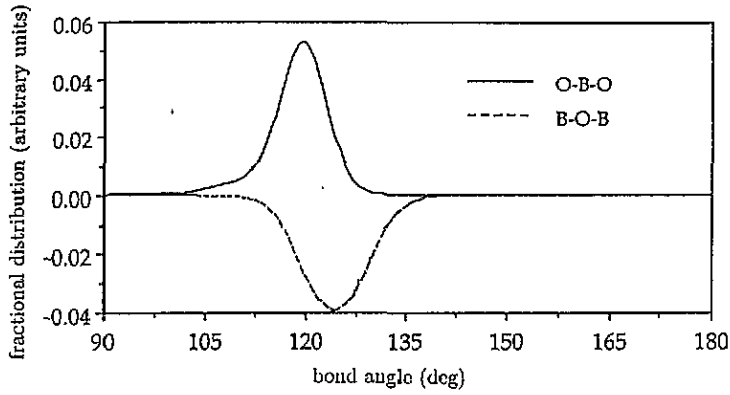

Figure 5. Calculated O–B–O and B–O–B bond-angle distribution for B_2O_3 glass at 300 K (using potential B1).

135°. Therefore, it is unlikely that the B–O–B angles are close to 160° in the vitreous structures. Moreover, if the potential favours wide B–O–B bond angles, it may prevent the generation of the boroxol rings. The pair-potential model with the full ionic charge results in excessive repulsion between the B–O bonds, as explained in part I of this study. This is almost certainly one of the reasons why previous MD studies could not generate boroxol rings. Inclusion of the three-body terms, combined with the partial charge and the Morse potential, seems to be very effective in modelling partial covalency in compounds such as B_2O_3. Detailed discussion of the comparison with x-ray and neutron scattering data will be given in section 3.3.

The next step was to relax this calculated structure to equilibrium at zero kelvin using the THBREL code [35], which is a lattice statics program. No significant changes in the dimensions of the simulation box occurred during the constant-pressure minimizations. The calculated bulk modulus of 11.4 GPa, compares with the experimental value of ≈15 GPa, while the calculated Young's modulus of 15.4 GPa, compares with experiment, ≈17 GPa.

Although all these results are very satisfactory, there is one problem: nine fourfold-

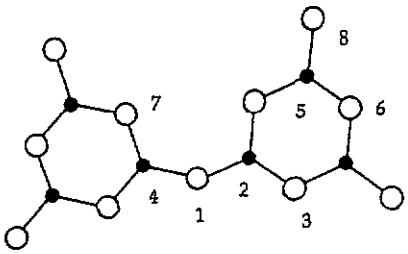

Peak	Kind of atoms	Designation on figure	Interatomic distance
D	B-O	1-2	1.37 Å
E	O-O	1-3	2.37
F	B-B	2-4, 2-5	2.43
G	B-O	2-6	2.74
H	B-O	2-7	Variable
I	B-O	2-7	3.63
J	O-O	3-8	4.10
K	O-O	3-7	Variable
L	O-O	1-8	4.75
M	B-O	4-6	5.25
N	B-O	5-7	Variable
O	B-O	4-8	Variable

Figure 6. Assignment of peaks in x-ray RDF for B_2O_3 glass [12].

coordinated boron atoms and nine threefold-coordinated oxygen atoms were observed. Many experiments suggest that almost all the boron atoms are threefold coordinated [36]. Furthermore, half of the six-membered rings contain more than one fourfold-coordinated boron atoms, that is, they are not true boroxol rings which are defined to have only threefold-coordinated boron atoms. The observations may be associated with the fact that the lattice energy of B_2O_3-II is calculated to be lower than that of B_2O_3-I, thus this potential would favour fourfold rather than the threefold coordination in some environments.

Finally, we attempted to include the 'aromatic stabilization' effects of boroxol rings in our MD simulations. The quantum-mechanical calculations suggested that such stabilization effects would not be so large as to control the geometries and networks [37–39]. To this end we roughly estimated the energy differences in the B–O bond in the monomer, dimer and trimer (boroxol ring), from the quantum-mechanically calculated energies, which was then expressed by the additional attractive Buckingham terms between the B–O interactions. These terms were then added to the B–O interactions present in boroxol rings. Even with these extra terms, there was no significant difference in the structures.

3.1.3. Simulation with transferable potential: summary. In applying the transferable potential model which can reproduce both crystal structures of B_2O_3 to the melt/quench MD simulations, we have obtained a vitreous structure containing six-membered rings (with 27% of the boron atoms), but which contains several fourfold-coordinated boron atoms which is inconsistent with much experimental data. The problem may be related to the fact that the difference between the lattice energies of the two polymorphs cannot be reproduced by this potential. We attempt to overcome this problem in the subsequent section.

3.2. New coordination-dependent potential model for polymorphic and vitreous structures

Clearly new procedures or new potentials must be derived in order to model satisfactory vitreous B_2O_3. Considering the latter we recall from part I of this study that potentials which could reproduce the two different crystal structures for B_2O_3 often failed to reproduce the difference in their lattice energies. In considering this difficult problem, the following points discussed in part I of this study of crystalline B_2O_3 should be considered.

(i) The LP simultaneous fitting procedures were applied to two B_2O_3 polymorphs after imposing the inequality conditions of their energies, but there was no feasible solution obtained as long as a transferable potential form was used.

(ii) Experimental data show that bond lengths strongly depend on coordination number; but not all the 'transferable' potentials can reproduce such differences well. In the case of B_2O_3 crystals, the variation in the B–O bond lengths with the coordination number around the boron atoms is reproduced well by the transferable potential, while the dependence of the bond lengths on the oxygen coordination are not expressed well by this potential. We note that potentials may be explicitly formulated so as to depend on the coordination number in a way similar to the bond strength concept defined by Pauling [40].

(iii) When the B–O potential alone was allowed to depend on the coordination number, there was no better solution than with the original transferable potential. However, when both the B–O and the O–O potentials were modified, better solutions (potential C1 and C2; listed in part I of this study) were found. These potentials cannot, however, as noted earlier, be implemented directly into the MD simulations, as they do not allow a continuous variation of the potential with coordination number. In view of these difficulties and observations we have developed a new more sophisticated potential which depends in a continuous manner on the coordination number.

The concepts used in this 'coordination-dependent potential' are as follows.

(i) The potential aims to treat the wide range of coordination states including the transient state around a bond breaking or rebonding state, by defining the 'bonding state function' F_b for each interaction:

$$F_b = \begin{cases} 1 & r < (R - D) \\ \{1 - \sin(\pi(r - R)/2D\} & (R - D) \leqslant r \leqslant (R + D) \\ 0 & (R + D) < r \end{cases} \tag{4}$$

where r is the distance between an oxygen atom and a boron atom. The range $R - D$ to $R + D$ represents the distances over which bond formation and breaking occur. At distances $r < (R - D)$ full B–O bonding is generated; for $(R - D) \leqslant r \leqslant (R + D)$ the extent of B–O bonding varies; when $(R + D) < r$, the B–O bonding is broken. The first derivative of this function is continuous when $r = R - D$ and $r = R + D$.

(ii) Next, the 'coordination function' F_c is defined for each atom:

$$F_c = \sum_i F_{bi} \tag{5}$$

where i is the sequential number of the B–O interactions around the atom concerned. When there is no transitional bonding state, F_c is the same as the coordination number. In this sense F_c can be said to be an 'extended' coordination number.

(iii) When the structure concerned has no transitional bonding, we use the potential set corresponding to the appropriate coordination state. However, when the structure has some transitional bonding, we interpolate between the two coordination states. The 'interpolation

factor' α is introduced. α is defined so that it becomes zero for one coordination state, while it becomes unity for the other state. The simplest procedure is to interpolate linearly, i.e. make α proportion to F_c. For example, when the potential V in the transitional state is interpolated from the potential V_2 in the twofold-coordinated state and the potential V_3 in the threefold-coordinated state, V becomes

$$\alpha = F_c - 2 \tag{6}$$

and

$$V(r) = (1-\alpha)V_2(r) + \alpha V_3(r) \tag{7}$$

(iv) These procedures are generally applied to the coordination environments of cations and/or anions. In the case of the B_2O_3 system, it is found that the change in the cation coordination can be expressed via the O–O interaction, while the change in the anion coordination cannot be well expressed with the B–B interaction. Therefore, only the changes in oxygen coordinations are treated using the procedure described above. For the three-body interactions, the respective three-body terms are applied to each coordination state.

(v) For the pair-potential term for the B–O interactions, the potential $V(r)$ (the Morse form) and its force $\partial V(r)/\partial r$ are calculated as follows

$$V(r) = (1-\alpha)V_2(r) + \alpha V_3(r) \tag{8}$$

$$\partial V(r)/\partial r = \{(1-\alpha)\partial V_2(r)/\partial r + \alpha \partial V_3(r)/\partial r\} + (\partial\alpha/\partial r)(-V_2(r) + V_3(r)) \tag{9}$$

where $V_2(r)$ and $V_3(r)$ are the pair-potential term for the twofold-coordinated oxygen and for the threefold-coordinated oxygen, and

$$\partial\alpha/\partial r = -\{\pi/(4D)\}\cos\{\pi(r-R)/2D\} \qquad \text{when } r < R-D \text{ or } r > R+D \tag{10}$$

$$\partial\alpha/\partial r = 0 \qquad \text{when } R-D < r < R+D. \tag{11}$$

(vi) For the pair-potential term for the O–O interactions, the potential $V(r)$ (Born–Mayer form) and its force $\partial V(r)/\partial r$ are calculated as follows. First, the general Born–Mayer form for the two oxygen atoms with the same coordination function F_c is

$$V(r) = A(F_c)\exp\{-r/\rho(F_c)\} \tag{12}$$

$$\partial V(r)/\partial r = (\partial A(F_c)/\partial r)\exp\{-r/\rho(F_c)\} + A(F_c)\partial[\exp\{-r/\rho(F_c)\}]/\partial r \tag{13}$$

$$A(F_c) = (1-\alpha)A_2 + \alpha A_3 \tag{14}$$

$$\rho(F_c) = (1-\alpha)\rho_2 + \alpha\rho_3 \tag{15}$$

where A_2, A_3, ρ_2 and ρ_3 are the A parameters and ρ parameters for twofold- or threefold-coordinated oxygen atoms. In the case of the B_2O_3 system, there are three interactions in the material: twofold-coordinated oxygen interacts with a second twofold-coordinated oxygen; twofold-coordinated oxygen with a threefold-coordinated oxygen; and threefold-coordinated oxygen with a second threefold-coordinated oxygen. These three sets of potential parameters can be derived from the two polymorphic structures of B_2O_3. After several tests of the LP fitting, it was found that only $A(F_c)$ should be varied, $\rho(r)$ being fixed in this system:

$$V(r) = A(F_c)\exp(-r/\rho) \tag{16}$$

$$\partial V(r)/\partial r = (\partial A(F_c)/\partial r)\exp(-r/\rho) - A(F_c)\exp(-r/\rho)/\rho \tag{17}$$

$$A(F_c) = (1 - \alpha)A_2 + \alpha A_3. \tag{18}$$

In the next step, the Born–Mayer form for the two oxygen atoms which have intermediate coordination is derived. As the simple geometric average did not work well as reported by Pertsin and Kitaigorodsky [41], a new interpolating function was introduced. When one atom has the coordination function F_{c-1} and the A parameter A_{-1}, and the other atom has the coordination function F_{c-2} and A parameter A_{-2}, the potential for the interaction between these two atoms is defined as follows:

$$A_{-1\&2} = \sqrt{(A_{-1}A_{-2})}[\{(\max(A_{-1}, A_{-2})/\min(A_{-1}, A_{-2}) - 1) - 1\}k + 1] \tag{19}$$

$$V(r) = A_{-1\&2} \exp(-r/\rho) \tag{20}$$

where k is the interpolation factor; k can be derived from the three sets of O–O parameters as explained above. When both oxygens have the same F_{c-3} and A_{-3}, $V(r)$ has a simple form of $A_{-3}\exp(-r/\rho)$. In this case the force $\partial V(r)/\partial r$ is approximated as follows:

$$\partial V(r)/\partial r = -A_{-1\&2}\exp(-r/\rho)/\rho. \tag{21}$$

To summarize, the 'coordination-dependent' potential has two main features. The first is that the change in the coordination environment affects the bond strength between atoms. It seems quite reasonable that as the number of the bonds increases, the bond strengths are reduced, as is the case in the well known Tersoff's potential [42]. The second is that the pair-potential terms change continuously between the two coordination states and the shape of the potential energy surface in the transient region can be adjusted smoothly by varying the R and D parameters, independently of the energy difference between the two polymorphs.

3.3. Application of 'coordination-dependent' potentials to MD

3.3.1. Selection of potential model. Two 'coordination-dependent' potential models which were modified from potentials C1 and C2 (see part I of this study) were used in MD simulations of the structures of vitreous B_2O_3. In order to apply the crystal potentials, C1 and C2, to the vitreous states, some parameters which were defined in the previous section were fixed as follows: $R = 1.8$ Å, $D = 2.0$ Å, and $k = 0.320$ and 0.295 for modified potentials C1 and C2 respectively.

The total number of atoms was 270 (108 boron atoms and 162 oxygen atoms). Although several runs with 480 atoms were undertaken, there were insignificant differences in the simulated structures. The time step in the calculations was 1 fs. To ensure more diffusion than the case described in section 3.1, the melting temperature was set at 5000 K. For the melting and quenching process, the initial crystal structure was kept at 5000 K for 10 000 steps. The system was quenched down to 1500 K in 500 K intervals, each of 1800 steps, after which it was quenched to 300 K in 100 K intervals, each of 900 steps. Finally, the system was kept at 300 K for 10 000 steps. 98% of the initial bonds were broken and rebonded with the other partners.

At first, constant-pressure simulations (using ambient pressures) were undertaken. The calculated coordination numbers, ring sizes and densities are shown in tables 1–3. Both potential models give simulated structures with a higher proportion of boroxol rings: 36% (modified potential C1) or 53% (modified potential C2) of boron atoms are present in boroxol rings values which are around the lower limit (40%) suggested by Johnson [3]. As the new potential models favours threefold rather than fourfold coordination (i.e. the energy of B_2O_3-I is lower than that of B_2O_3-II), the fourfold-coordinated boron atoms are

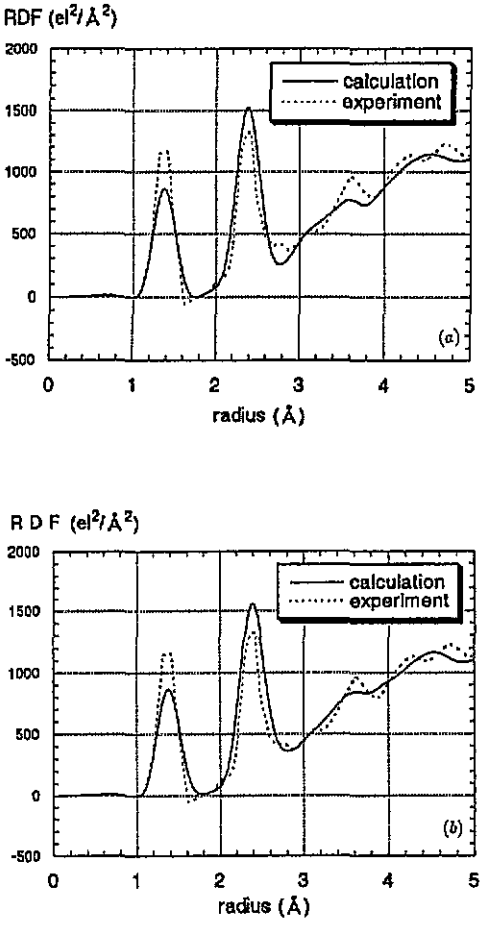

Figure 7. X-ray RDF for B_2O_3 glass at 300 K: (a) modified potential C1; (b) modified potential C2.

no longer present. However, one new problem appears: the final calculated density is too low compared with that found experimentally. Thus, although these potential models successfully generate boroxol rings, it would still appear to be difficult for the present MD method to reproduce the whole structural transformation during the melting process at high temperatures so as to reproduce correctly the density.

Next, therefore, the constant-volume method was applied using the same potential sets, in order to study the structural transformations keeping the experimental density. The calculated coordination numbers and ring sizes are shown in tables 1 and 2.

The percentage of the boron atoms consisting of the six-membered rings (25% for modified potential C1; 42% for modified potential C2) was lower than that observed with the constant-pressure calculations, and fourfold-coordinated boron atoms were observed in the simulations using potential C2.

To summarize, using the constant-pressure method these new potentials generated almost the same percentage of boroxol rings as that estimated from the experiment, but they resulted in a lower density (i.e. they may have different intermediate range order), while using the constant-volume method the simulations generated fourfold boron atoms, although they necessarily kept the experimental density. It is clearly difficult therefore to realize both the

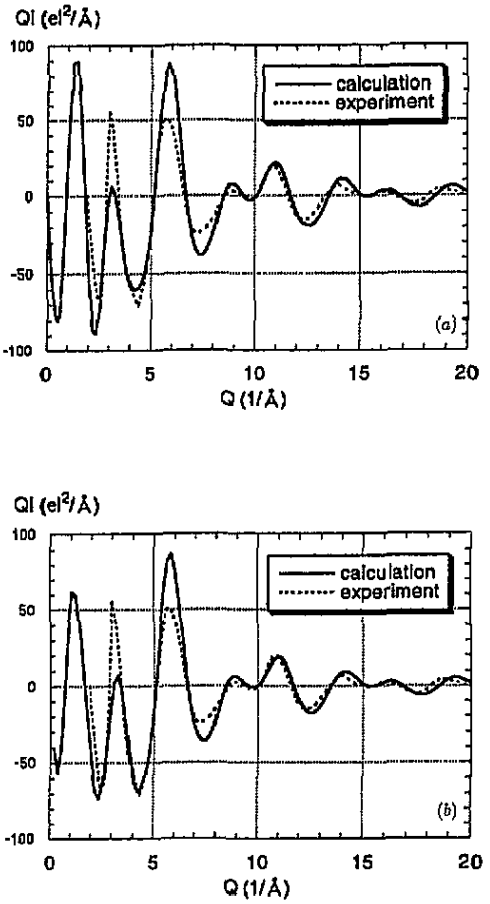

Figure 8. X-ray interference function for B_2O_3 glass at 300 K: (a) modified potential C1; (b) modified potential C2.

high proportion of the boroxol rings and the experimental density at the same time.

3.3.2. Comparison with x-ray diffraction and neutron scattering data. We have compared the calculated vitreous structures with the x-ray diffraction data of Mozzi and Warren [12] and the neutron scattering data of Johnson *et al* [3]. From the calculated structures using modified potentials C1 and C2, the RDFs and interference functions were simulated and compared with those obtained from the experimental data. In order to make comparison with the latter, the same filtering and conversion procedures were used.

The relation between the RDF (=$G(r)$) and the interference function (=$QI(Q)$) is given as:

$$G(r) = 1 + \{1/(2\pi^2\rho_0)\} \int_0^{Q_{max}} QI(Q) \sin(Qr)\, dQ \tag{22}$$

where r and Q are the real-space and reciprocal vectors, $I(Q)$ and r_0 indicate the measured intensity and the average number density.

For the x-ray diffraction data, two points must be carefully noted. The first is that the peak at 2.8 Å in the x-ray RDF data in the original paper of Mozzi and Warren [12]

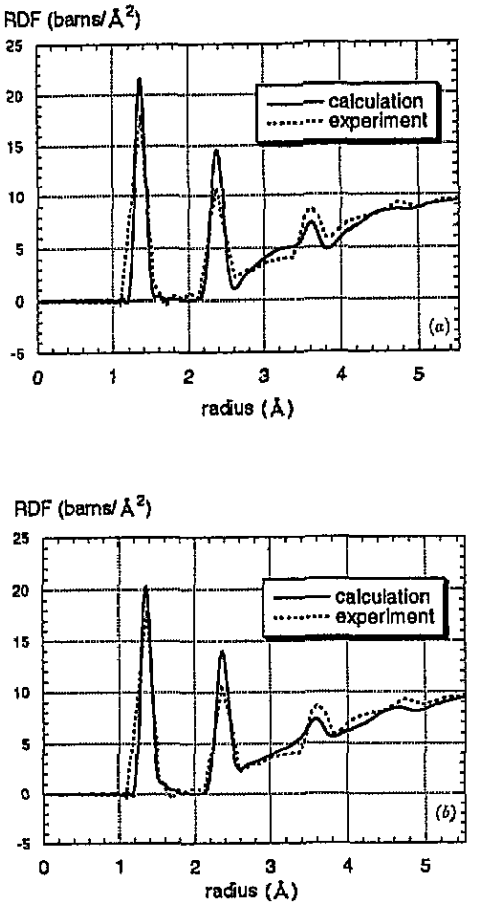

Figure 9. Neutron RDF for B_2O_3 glass at 300 K: (a) modified potential C1; (b) modified potential C2.

appeared to be absent after a retransformation of the interference function using a window, as noted by Johnson *et al* [3]. Therefore, the comparison with the interference function may be better than that with the RDF. The other is that the atomic form factors are dependent on the x-ray wavelength and the atomic charge state, and it is not easy to use precise values. Verhoef and den Hartog [27] demonstrated that the difference in the approximation of the atomic form factors considerably affected the height of the first and second peaks within 6 Å in the interference functions. Here, the interpolating function appropriate for neutral atoms was used from the *International Tables for X-ray Crystallography* [43].

For the neutron scattering data, the atomic scattering factors are independent of Q (wavevector), and the experimental intensity was measured up to 40 Å^{-1}. The neutron data may be more suitable for comparison with the calculated results, and therefore more emphasis is placed on the latter data in this paper.

The calculated RDFs and the interference functions for the x-ray diffraction data are shown in figures 7 and 8; those for the neutron scattering data are shown in figures 9 and 10.

The calculated RDFs and the interference functions for both potentials agree reasonably with both x-ray and neutron experimental data. For the calculated RDF appropriate to the

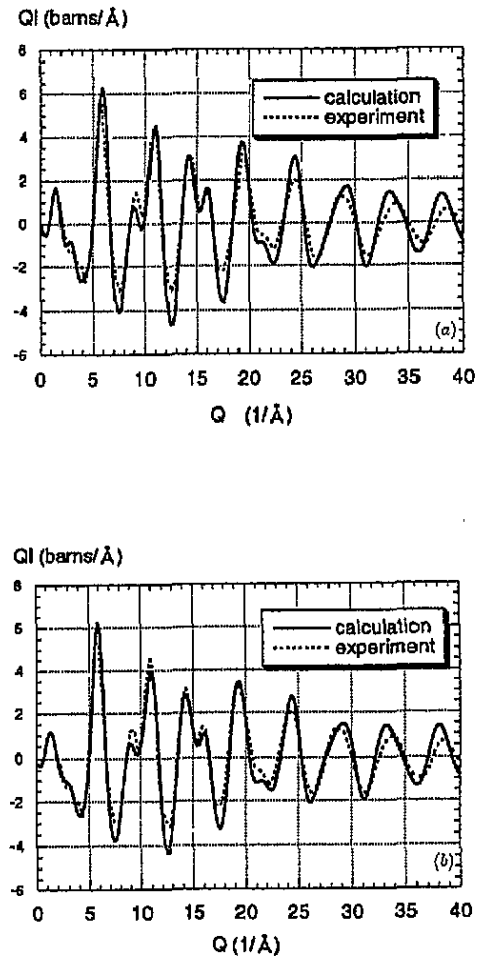

Figure 10. Neutron interference function for B_2O_3 glass at 300 K: (a) modified potential C1; (b) modified potential C2.

neutron scattering data, the peaks at 1.37 Å and 2.37 Å agree with experiment, although their heights are still a little too large. However, two small and broad peaks around 3 Å in the experimental data are not distinguishable in the calculated RDF. This is possibly due to the relatively small proportion of boroxol rings, as it is certain that boroxol rings result in these two peaks (G and H).

For the interference function of the neutron scattering data, the shapes of the branches in the peaks around 10 $Å^{-1}$ and 15 $Å^{-1}$ agree very well with the experimental data. All these features seem to be related to the structures of boroxol rings and to originate from the intermediate-range rather than the short-range order. This point is discussed further in the following section.

3.3.3. Short-range and intermediate-range order. Our calculated results showed that models including six-membered rings can reproduce the x-ray and neutron scattering data well, as many previous experimental studies have suggested. However, it is very difficult to discuss the intermediate-range order present in vitreous structures using only experimental

data. In contrast, not only the short-range but also the intermediate-range order is available from analysis of the calculated structures.

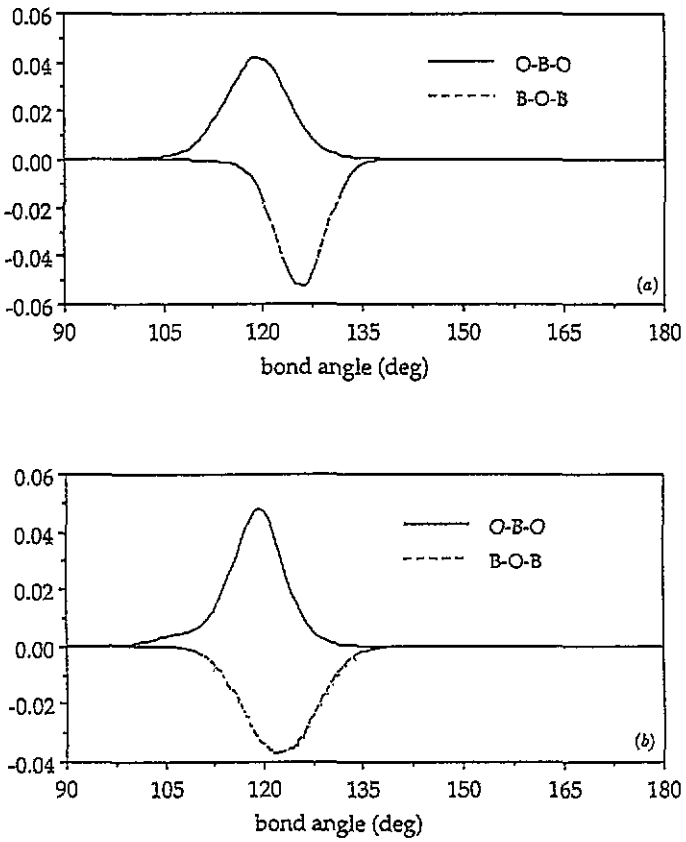

Figure 11. Bond-angle distribution in calculated vitreous structures at 300 K: (a) modified potential C1; (b) modified potential C2.

Firstly, the O–B–O and the B–O–B bond angle distributions (BADs) at 300 K in the cases of modified potentials C1 and C2 are shown in figure 11. As their peaks are more easily distinguished and compared at zero kelvin, all the BAD data are calculated at zero kelvin (i.e. after energy minimization) and are shown in figures 12–14. For the sake of comparison we show the energy-minimized structures from the experimental structures of B_2O_3-I and $Cs_2O{\cdot}9B_2O_3$ and the calculated structures for the pseudo-super-crystals based on the latter studies (see part I of this study) and the MD results all at zero kelvin. They exhibit several peaks around 120° for the O–B–O bond angles, and two groups of peaks around 120° and 128° for the B–O–B bond angles. For the latter it is interesting to note that the peak around 120° corresponds to the angles within the boroxol rings, while that around 128° corresponds to the angles outside the rings. The latter value agrees with that estimated from the NMR experiment by Jellison [26]; the B–O–B angles for the oxygen atoms not included in the boroxol rings have a narrow distribution (rms deviation ~1.7°) centred around either 134.6° or 128.1° (which cannot be distinguished by experiment). These values contrast with the much larger angles calculated from the pair-potential models, as explained in section 2.2.

The existence of boroxol rings and the B–O–B angles of 128° outside the boroxol

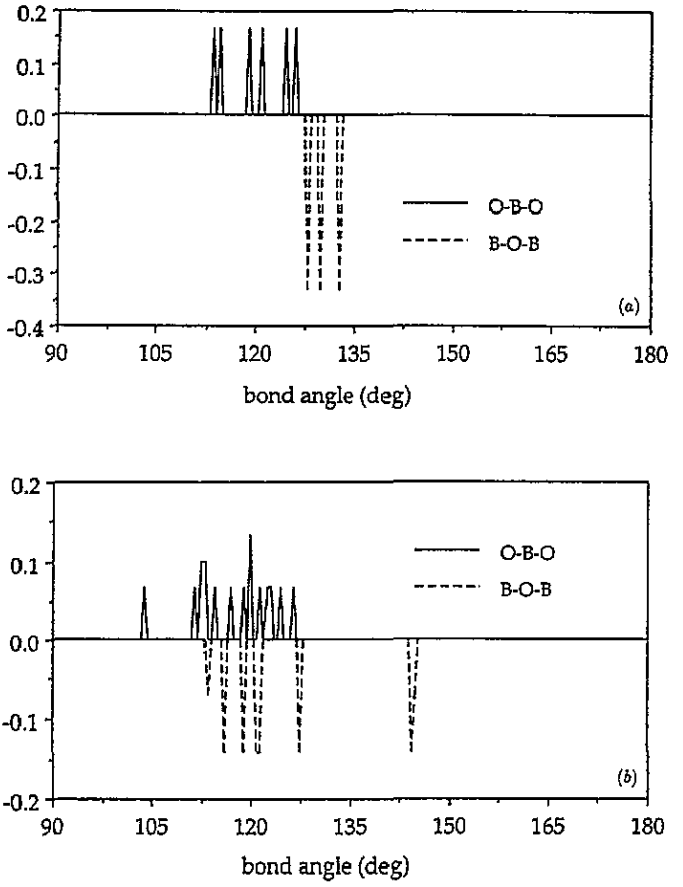

Figure 12. Bond-angle distribution in B_2O_3-I and $Cs_2O \cdot 9B_2O_3$ crystals at 0 K: (a) B_2O_3-I; (b) $Cs_2O \cdot 9B_2O_3$.

rings is clearly demonstrated. However, if these are randomly connected, the structural model cannot reproduce the experimental density [13]. In order to analyse the topology of the connections, we need the torsion angle distribution (TAD) between the BO_3 triangles, and between the BO_3 triangle and the B_3O_6 ring, or between the B_3O_6 rings. (To define the torsion angles between two planes, we consider each plane as defined by the three oxygen atoms present in the BO_3 triangles whether within or outside the B_3O_6 rings.) The BO_3 triangles with more than one fourfold-coordinated boron atoms were excluded from the analysis. The calculated results are shown in figure 15–21. It must be noted that all the peaks are sharp, because they are calculated at zero kelvin and confined to several equilibrium values.

The TAD in the crystal of B_2O_3-I has two peaks of 7° and 74° (figure 15(a)). It is interesting to note that two triangles even on the same chain are twisted by 7°, while those on the different chains, by 74°, which is close to the perpendicular. These contrast with the quantum-chemically calculated value of 29.4° for the $(HO)_2B–O–B(OH)_2$ molecule [38]. For the TAD in the crystal of $Cs_2O \cdot 9B_2O_3$, two of the peaks are almost the same as those in B_2O_3-I and the other has a peak around 44° (figure 15(b)). The latter value is quite close to the quantum-chemically calculated value of 32.2° obtained for $(HO)_2B_3O_3–O–B_3O_3(OH)_2$ [38]. These two results may mean that the B_2O_3 systems do not favour a layer structure

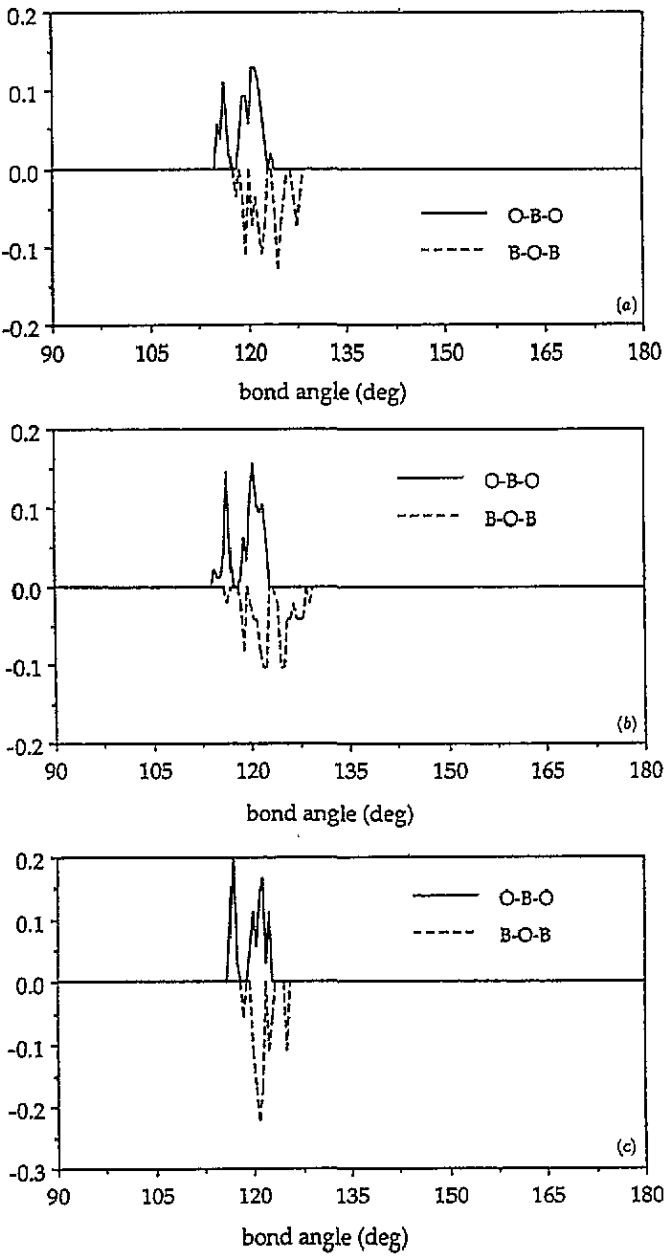

Figure 13. Bond-angle distribution in pseudo-super-crystals at 0 K (using modified potential C2): (a) B_2O_3-c; (b) B_2O_3-d; (c) B_2O_3-a.

and they prefer the large torsion angle which does not appear in the molecular state and is apparently caused by crystal effects.

The calculated structures of pseudo-super-crystals also have large torsion angles (figures 16–18), as do the structures calculated by the MD method, although they also have other peaks at lower angles (figures 19 and 20). It is interesting to note that in the calculated structures, the torsion angles within the B_3O_6 rings exhibit the twisted angles from 10° to

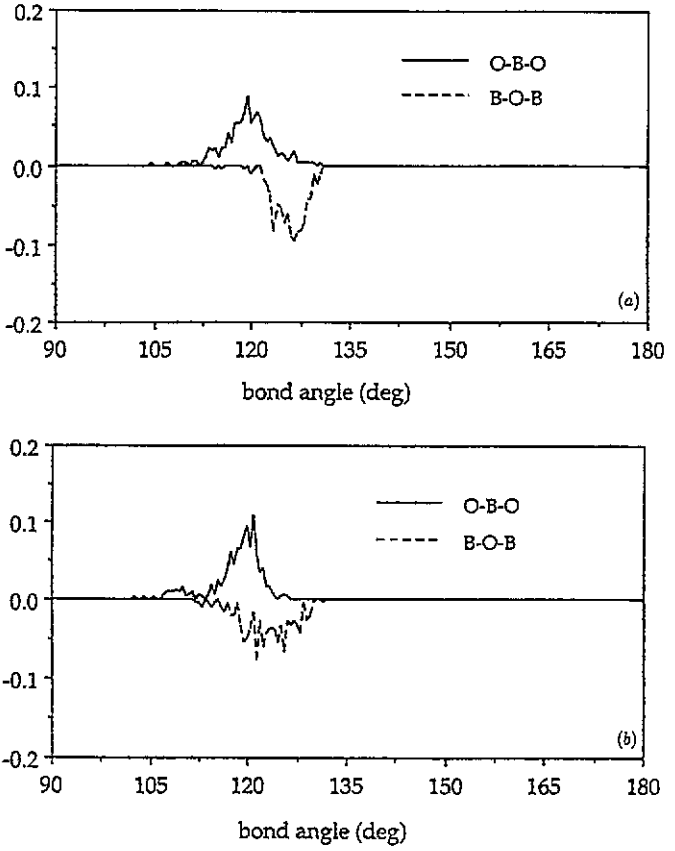

Figure 14. Bond-angle distribution in calculated vitreous structures at 0 K: (a) modified potential C1; (b) modified potential C2.

30° (figure 21), indicating that the three oxygen atoms outside the B_3O_3 rings do not lie on the same plane as the B_3O_3 rings and that they are easily distorted. The hypothesis that a considerable proportion of the torsion angles would be as large as 74° and that the oxygen atoms outside the rings do not lie in the same plane as those within the rings may explain the experimental density, in contrast to the lower density obtained from the models base on the randomly connected boroxol rings. Appreciation of this point, which we described using the term 'interlocking structure' for $Cs_2O \cdot 9B_2O_3$ in part I of this study, may lead to accurate models for the intermediate-range order in vitreous B_2O_3 structures.

3.3.4. Lattice dynamics simulation. The vitreous structure calculated using modified potential C2 was energy minimized and its lattice dynamical properties were calculated employing the GULP code [44], as described in part I of this study. The calculated vibrational densities of states at 300 K are shown in figure 22. For the sake of comparison, calculated densities of states for crystalline B_2O_3-I and the two 'computer-synthesized' crystals, which were reported in part I of this study, are also shown in figure 23. The vitreous structures have two peaks at 740 cm^{-1} and 805 cm^{-1} which correspond respectively to peak (A) in B_2O_3-I and peak (B) in B_2O_3-a, and indeed the structure appears to have features intermediate between these two crystalline forms. Furthermore, the vitreous models

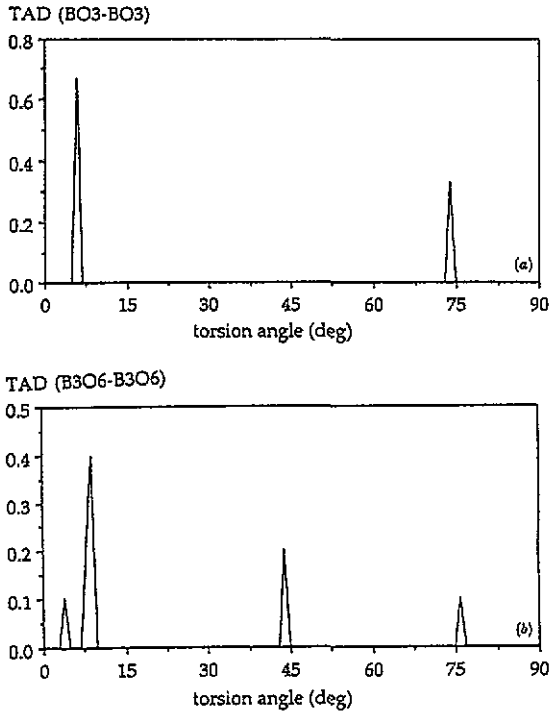

Figure 15. Torsion angle distribution in B_2O_3-I and $Cs_2O \cdot 9B_2O_3$ crystals at 0 K: (a) B_2O_3-I; (b) $Cs_2O \cdot 9B_2O_3$.

have the other higher peak (C) of 775 cm^{-1}, which does not exist either in the B_2O_3-I or B_2O_3-a. This calculated structure still contains several BO_4 tetrahedra, and peak (C) is assigned to a vibration of the six-membered rings with one or two BO_4 tetrahedra, as noted by Konijnendijk and Stevels [45] in their study of the spectra of the alkali borate crystals. To summarize, the success of our model in reproducing the peak around 805 cm^{-1} strongly supports the existence of boroxol rings, as suggested by the Raman experiments.

3.3.5. Structural transformation in the glass formation. In our LDF calculations [46, 47] of crystalline B_2O_3 the structural transformation from the BO_3 triangular structural unit to the BO_4 tetrahedral unit was observed to occur smoothly without breaking any B–O bonds. However, such a smooth transformation without bond breaking seems to be topologically impossible between the independent BO_3 triangular structural unit and the B_3O_6 boroxol ring unit.

Here, we investigated the nature of the structural transformations in the melting and quenching simulations. Two types of transformations were observed. In the first at 1500 K, two thirds of the boron atoms have twofold coordination, and as the system is quenched, the twofold-coordinated boron atoms bond with the non-bridging or the twofold-coordinated oxygen atoms (see figure 24, (a) and (b)). In the latter case, after the generation of a six-membered ring, one original B–O bond is broken. In the second, below 1000 K, the threefold-coordinated boron atoms bond with the fourth oxygen atom. The transient state has fourfold-coordinated boron and threefold-coordinated oxygen atoms (see figure 24(c)). Then after the generation of a six-membered ring, two new B–O bonds are created.

It is interesting to note that Mackenzie [48] proposed non-bridging –B=O groups

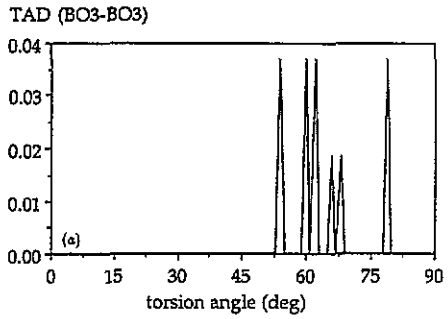

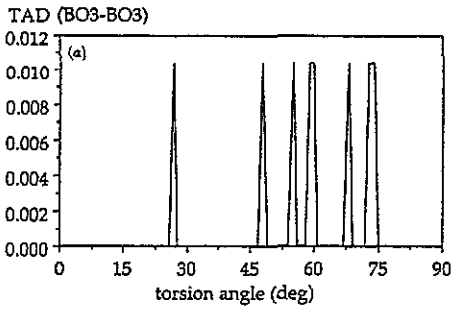

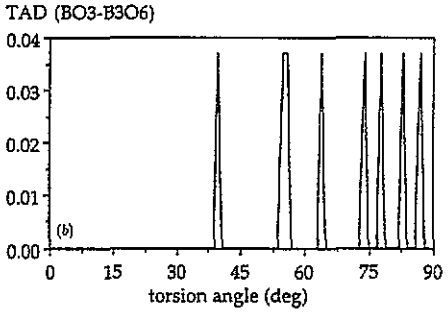

Figure 16. Torsion angle distribution in pseudo-super-crystal B_2O_3-c at 0 K (using modified potential C2): (a) between BO_3 triangles; (b) between BO_3 triangle and B_3O_6 ring.

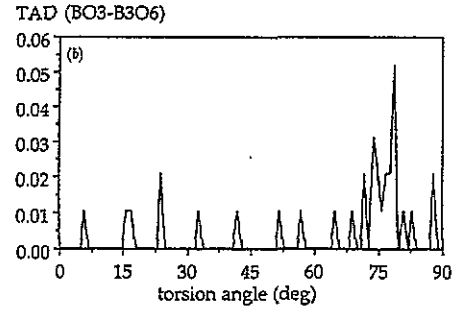

Figure 17. Torsion angle distribution in pseudo-super-crystal B_2O_3-d at 0 K (using modified potential C2): (a) between BO_3 triangles; (b) between BO_3 triangle and B_3O_6 ring.

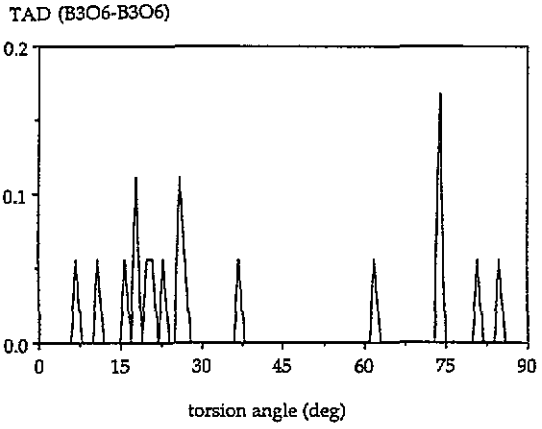

Figure 18. Torsion angle distribution in pseudo-super-crystal B_2O_3-a at 0 K (using modified potential C2). Angles smaller than 45° are all between the same B_3O_6 rings. Angles larger than 45° are all between the different B_3O_6 rings.

were present as higher-energy species in molten B_2O_3, while Krogh-Moe [49] proposed fourfold-coordinated boron and threefold-coordinated oxygen atoms. Both hypotheses were suggested independently. However, they correspond to our results and we can now distinguish between them: the first is the 'high-temperature structural transformation', while

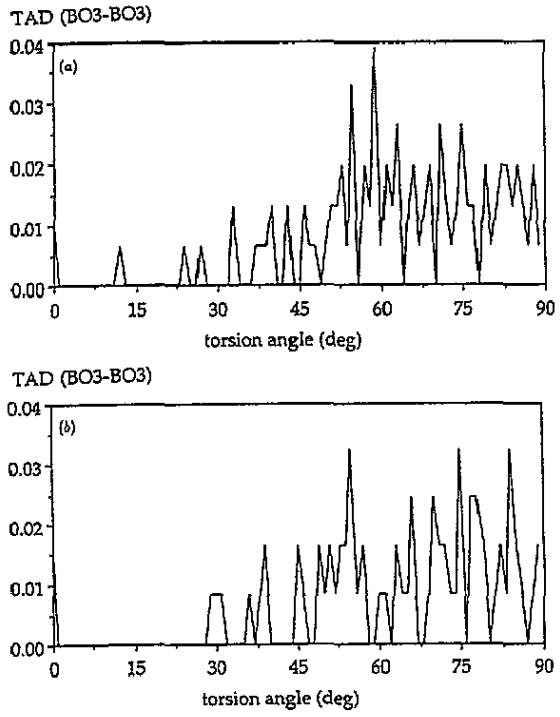

Figure 19. Torsion angle distribution in calculated vitreous structure using modified potentials *C1 and C2 at 0 K. (a) C1; (b) C2. All angles are between* BO_3 *triangles.*

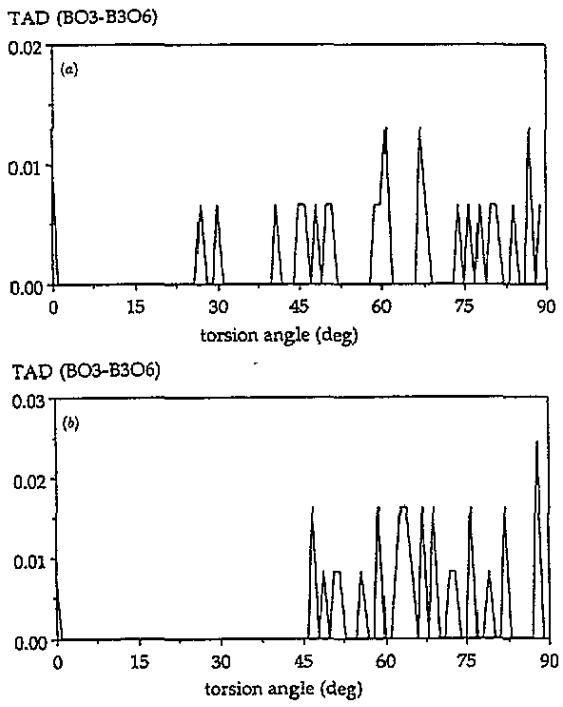

Figure 20. Torsion angle distribution in calculated vitreous structure using modified potentials C1 and C2 at 0 K. (a) C1; (b) C2. All angles are between BO_3 triangle and B_3O_6 ring.

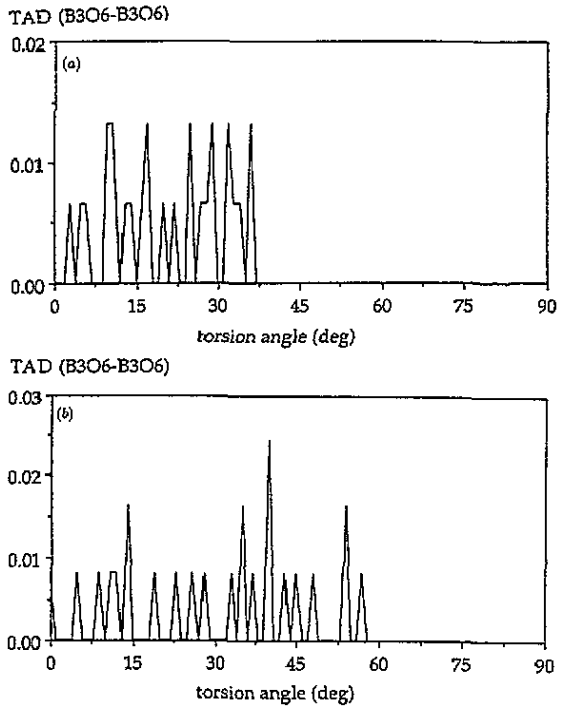

Figure 21. Torsion angle distribution in calculated vitreous structure using modified potentials C1 and C2 at 0 K. (a) C1; (b) C2. All angles are within B_3O_6 rings.

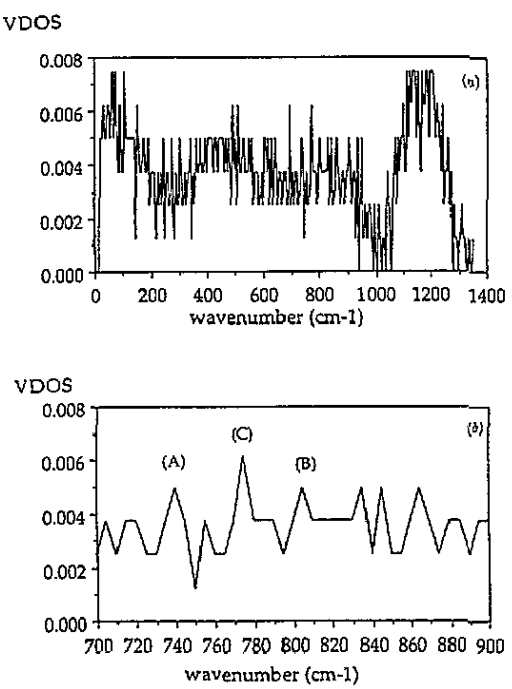

Figure 22. Vibrational density of states in calculated vitreous structure using modified potential C2 at 0 K. See the text for (A), (B) and (C).

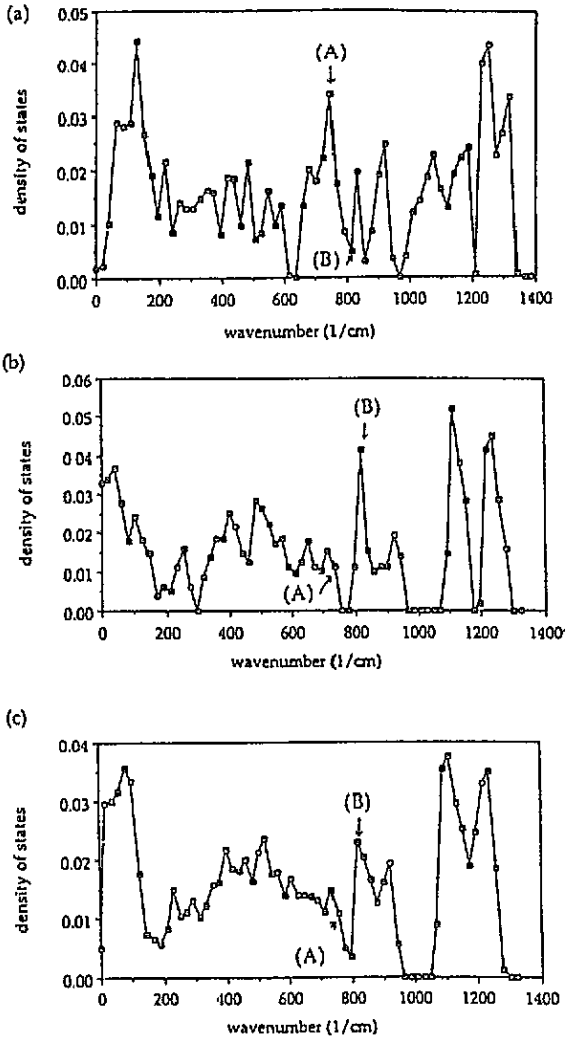

Figure 23. Calculated densities of states for (a) crystalline B_2O_3-I, (b) pseudo-super-crystal B_2O_3-a, and (c) pseudo-super-crystal B_2O_3-d. See text for (A), (B) and (C).

the second is the 'low-temperature structural transformation'. It is also interesting to note that the latter hypothesis may explain one of the reasons why a proportion of the fourfold-coordinated boron was always observed in our MD simulations even when the coordination-dependent potential model was used; the transient structures would be frozen before finding the appropriate bonding partners because of the rapid quench rates.

4. Estimation of the ratio of boroxol rings to independent BO_3 units

One of the major concerns in our MD simulations is the ratio of the boroxol rings to the independent BO_3 units. The NMR study [26] and the neutron diffraction study [3] estimated the fraction of the boron atoms included in the boroxol rings as $82 \pm 8\%$ and $60 \pm 20\%$ respectively. The MD simulated structures contained a 30–50% fraction of the boroxol rings. This discrepancy almost certainly arises from the limitations of our MD studies,

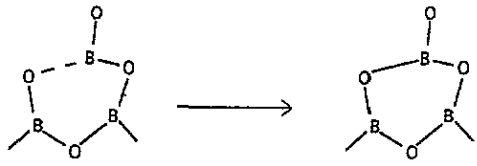

(a) 2 fold coordinated boron + non-bridging oxygen

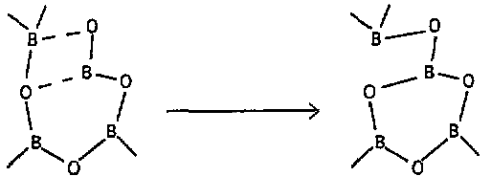

(b) 2-fold coordinated boron + 2 fold coordinated oxygen

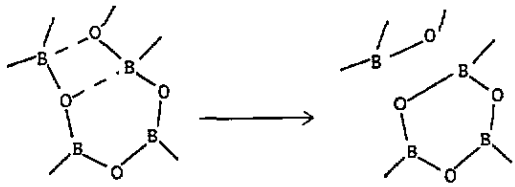

(c) 3 fold coordinated boron + 2 fold coordinated oxygen

Figure 24. Schematic diagram for structural transformation observed in MD simulations.

which arise from three main sources.

The first is provided by finite-size effects. When the simulated system is a perfect crystal or its structure has only short-range order, this limitation may not be too serious. However, when the system is disordered, the simulation box must be large enough that the artificial periodicity does not significantly affect the results. For Lennard-Jones-type potentials the calculations with as many as one million particles may be possible. However, for the case of oxide materials the more sophisticated potentials needed for accurate simulations do not allow such large calculations. The main reason is that for ionic materials the calculation of the long-range Coulombic terms is computationally expensive, even when the efficient Ewald summation procedure is used. The other reason is that in order to express covalent effects the potentials have to include three-body and in some cases four-body terms; and these terms require much larger numbers of interactions.

The second limitation is the finite real time sampled in the simulations, which is rarely more than ~1 ns in modern simulations. Most physical properties are calculated by averaging over the simulation. But the period of real time sampled may be insufficient to model the processes occurring in the real system. Thus, in glass formation, the quench rate is crucial in controlling the final vitreous structures. MD quench rates are several orders of magnitude greater than the real rates.

The third limitation is the accuracy and transferability of the potential model. As argued in both this and the previous paper, the present potentials represent an advance on these previously used but there may still be room for further refinement using spectroscopic data.

Of course, the ideal solution would be to remove the necessity of relying on interatomic potentials by using *ab initio* MD techniques [49]. At present, however, such methods are not viable for long-timescale runs on the large complex systems investigated here.

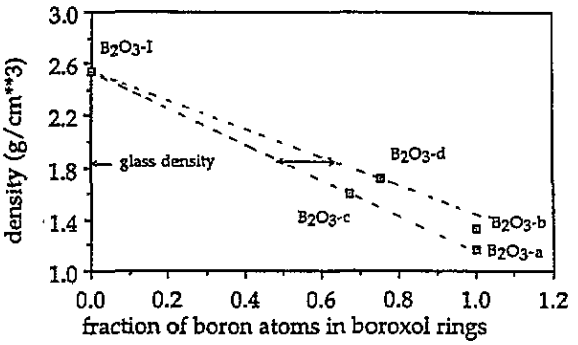

Figure 25. Relation between fractions of boron atoms contained in boroxol rings and densities.

One of the most useful clues in unravelling these complexities may be the glass density which strongly depends on the structure. After the construction of the possible polymorphs of crystalline B_2O_3 shown in part I of this study, we now have one experimental density for B_2O_3-I and four simulated densities for B_2O_3-a, B_2O_3-b, B_2O_3-c and B_2O_3-d. The relation between the fractions of the boron atoms contained in the boroxol rings and the densities are plotted in figure 25. We note that the bond lengths and angles in these structures are all very similar. So the changes in density are due to changes in the intermediate-range order. There is a clear correlation between the density and the boroxol ring content, although there is appreciable variance in the correlation. However, the fraction which corresponds to the glass density can be estimated as 50–64%. When the calculated structures explained in this paper and the related study of crystalline B_2O_3 are taken into account, one of the possible crystalline analogues for vitreous B_2O_3 may be the disordered structure based on B_2O_3-c and B_2O_3-d, with some B_3O_6 rings replaced with BO_3 triangular units.

Several MD simulations which started from the structure of pseudo-super-crystal B_2O_3-d (a good candidate for vitreous B_2O_3) were also performed. The system was melted and then quenched in the same way as explained in section 3. The final vitreous structure turned out to be almost the same as those calculated in section 3. An improvement was not observed, because the system probably lost most of its initial structure.

5. Conclusions

The transferable potentials derived in the part I of this study clearly enjoyed considerable success when applied to modelling B_2O_3. Moreover, the new coordination-dependent potential, when implemented in constant-pressure simulations, successfully reduced the proportion of the fourfold boron atoms and increased the proportion of the six-membered rings closer to the lower limit (40%) of that estimated by the neutron study, although the calculated densities became too low. In the constant-volume calculations, the proportion of the six-membered rings was reduced and fourfold boron atoms appeared. However, the calculated structures agree with the RDFs and interference functions derived from the x-ray diffraction data and with the neutron scattering data. It is interesting to note that all these structural models have one important feature concerning the intermediate-range order, namely, that a considerable proportion of the torsion angles between the BO_3 triangles,

between the BO_3 triangle and the B_3O_6 ring and between the B_3O_6 rings are around 74°, although the MD simulated structures contain smaller torsion angles. This feature seems to be important in reproducing the experimental density without the presence of fourfold-coordinated boron atoms.

Regarding the vibrational properties, as the calculated structure contained fourfold-coordinated boron atoms, the lattice dynamics simulation of the structure exhibited two characteristic peaks seen in the Raman spectra; the first is at 805 cm^{-1} and is due only to the boroxol ring with BO_3 triangles; and the other is at 775 cm^{-1} and corresponds to the six-membered ring with one or two BO_4 units.

These MD studies using the new potential models demonstrate structural transformations in glass formation and confirm the existence of the boroxol rings, in contrast with the other MD studies employing the pair-potentials. However, there are several fourfold-coordinated boron atoms remaining and the proportion of the boroxol rings is still smaller than that estimated by experiments. There are three possible explanations: the first concerns the effect of the finite simulation time as explained in section 4. Although our new potential model favours the threefold-coordinated environment rather than the fourfold one, the simulation must have sufficient time for the structure to rearrange during the quench process, and the present timescale may not be sufficient. The second is the finite-size effect explained in section 4. As the B_2O_3 system has much more pronounced intermediate-range order than in the other oxide materials, the simulation box may need to be much larger. The third concerns the accuracy of the potential models. The new potentials could reproduced two crystal structures well, but it may require still further improvement using spectroscopic data and properties of the molten state.

Although MD studies based on the pseudo-super-crystal structures were not successful, future work based on these structures may lead to the possibility of simulating more accurate vitreous structures. A final, key feature of our analysis is the estimation of the fraction of boron atoms present in boroxol rings as 50–64%, from the relation between the calculated structures and densities for polymorphs.

Acknowledgments

We are gratefully acknowledge many useful discussions with Drs B Vessal, E Hernandez and J D Gale. The calculations used computer facilities provided by SERC.

References

[1] Pye L D, Frechett V D and Kreidl N J ed 1978 *Borate Glasses: Structure, Properties, Applications* (New York: Plenum)
[2] Zachariasen W H 1932 *J. Am. Chem. Soc.* **54** 3841
[3] Johnson P A V and Wright A C 1982 *J. Non-Cryst. Solids* **50** 281
[4] Abe T 1952 *J. Am. Ceram. Soc.* **35** 284
[5] Eversteijn F E, Stevels J M and Waterman H I 1960 *Phys. Chem. Glasses* **1** 123
[6] Huggins M L and Abe T 1957 *J. Am. Ceram. Soc.* **40** 287
[7] Krogh-Moe J 1969 *J. Non-Cryst. Solids* **1** 269
[8] Borelli N F and Su G J 1963 *Phys. Chem. Glasses* **4** 206
[9] Fajans K and Barber S W 1952 *J. Am. Chem. Soc.* **74** 2761
[10] Goubeau J and Keller H 1953 *Z. Anorg. Chem.* **272** 303
[11] Elliot S R 1978 *Phil. Mag.* B **37** 435
[12] Mozzi R L and Warren B E 1970 *J. Appl. Crystallogr.* **3** 251
[13] Bell R J and Carnevale A 1981 *Phil. Mag.* B **43** 389
[14] Woodcock L V, Angell C A and Cheeseman P 1976 *J. Chem. Phys.* **65** 1565

[15] Soules T F 1979 *J. Chem. Phys.* **71** 4570
[16] Soules T F 1980 *J. Chem. Phys.* **73** 4032
[17] Soules T F and Varshneya A K 1981 *J. Am. Ceram. Soc.* **64** 145
[18] Soppe W, van der Marel C, van Gunsteren W F and den Hartog H W 1988 *J. Non-Cryst. Solids.* **103** 201
[19] Soppe W and den Hartog H W 1988 *J. Phys. C: Solid State Phys.* **21** L689
[20] Soppe W and den Hartog H W 1989 *J. Non-Cryst. Solids* **108** 260
[21] Amini M, Mitra S K and Hockney R W 1981 *J. Phys. C: Solid State Phys.* **14** 3689
[22] Abramo M C and Pizzimenti G 1986 *J. Non-Cryst. Solids* **85** 233
[23] Xu Q, Kawamura K and Yokokawa T 1988 *J. Non-Cryst. Solids* **104** 261
[24] Hirao K and Soga N 1985 *J. Am. Ceram. Soc.* **68** 515
[25] Inoue H, Aoki N and Yasui I 1987 *J. Am. Ceram. Soc.* **70** 622
[26] Jellison G E Jr, Panek L W, Bray D J and Rouse G B Jr 1977 *J. Chem. Phys.* **66** 802
[27] Verhoef A H and den Hartog H W 1992 *J. Non-Cryst. Solids* **146** 267
[28] Gurr G E , Mongomery D W, Knutson C D and Gorres B T 1970 *Acta Crystallogr.* B **26** 906
[29] Prewitt C T and Shannon R D 1968 *Acta Crystallogr.* B **24** 869
[30] Allen M P and Tildesley D J 1989 *Computer Simulation of Liquids* (Oxford: Clarendon)
[31] Walker J R 1982 *Computer Modelling of Solids (Springer Lecture Notes in Physics 166)* ed C R A Catlow and W C Mackrodt (Berlin: Springer)
[32] Vessal B, Leslie M and Catlow C R A 1989 *Mol. Simul.* **3** 123
[33] Ewald P P 1921 *Ann. Phys., Lpz.* **64** 253
[34] Macedo P B, Capps W and Litovitz T A 1966 *J. Chem. Phys.* **44** 3357
[35] THBREL was developed by M Leslie at Daresbury Laboratory, and is available through the CCP5 library.
[36] Griscom D L 1978 *Borate Glasses: Structure, Properties, Applications* ed L D Pye, V D Frechett and N J Kreidl (New York: Plenum)
[37] Snyder L C 1978 *Borate Glasses: Structure, Properties, Applications* ed L D Pye, V D Frechett and N J Kreidl (New York: Plenum)
[38] Uchida N, Maekawa T and Yokokawa T 1985 *J. Non-Cryst. Solids* **74** 25
[39] Uchida N, Maekawa T and Yokokawa T 1986 *J. Non-Cryst Solids* **85** 290
[40] Pauling L 1960 *The Nature of the Chemical Bond* 3rd edn (Ithaca, NY: Cornell University Press)
[41] Pertsin A J and Kitaigorodsky A I 1987 *The Atom–Atom Potential Method: Application to Organic Molecular Solids* (Berlin: Springer)
[42] Tersoff J 1986 *Phys. Rev. Lett.* **56** 632
[43] *International Tables for X-ray Crystallography* 1962 vol III (Birmingham: Kynoch)
[44] Gale J D 1993 private communication
[45] Konijnendijk W L and Stevels J M 1978 *Borate Glasses: Structure, Properties, Applications* ed L D Pye, V D Frechett and N J Kreidl (New York: Plenum)
[46] Takada A, Catlow C R A, Lin J S, Price G D, Lee M H, Milman V and Payne M C 1995 *Phys. Rev.* B **51** 1447
[47] Takada A 1994 *PhD Thesis* University College London
[48] Mackenzie J D 1959 *J. Phys. Chem. Solids* **63** 1875
[49] Krogh-Moe J 1960 *Phys. Chem. Glasses* **1** 26
[50] Car R and Parrinello M 1985 *Phys. Rev. Lett.* **55** 2471